

# PROPERTIES OF SURFACE AND INTERNAL SOLITARY WAVES

Kei Yamashita<sup>1</sup> and Taro Kakinuma<sup>2</sup>

Numerical solutions of surface and internal solitary waves are obtained through a new method, where advection equations on physical quantities including surface/interface displacements and velocity potential are solved to find convergent solutions by applying the Newton-Raphson method. The nonlinear wave equations derived using a variational principle are adopted as the fundamental equations in the present study. Surface and internal solitary waves obtained through the proposed method are compared with the corresponding theoretical solutions, as well as numerical solutions of the Euler equations, to verify the accuracy of solutions through the proposed method especially for internal solitary waves of large amplitude progressing at a large celerity with a flattened wave profile. Properties of surface and internal solitary waves are discussed considering vertical distribution of horizontal and vertical velocity, as well as kinetic and potential energy. Numerical simulation using a time-dependent model has also been performed to represent propagation of surface and internal solitary waves with permanent waveforms.

*Keywords: solitary wave; internal wave; large amplitude; nonlinear wave equation; advection equation*

## INTRODUCTION

Solitary waves of large amplitude play an important role in nearshore zones, such that the characteristics of surface solitary waves have been examined by many researchers, e.g. Longuet-Higgins and Fenton (1974). On the other hand, in a lake or the ocean where density stratification is well developed, internal solitary waves are observed (e.g. Stanton and Ostrovsky, 1998; Duda et al., 2004). In particular, internal waves of large amplitude have great effects on environments through transportation of nutrient salts, variation of water temperature, etc. Internal solitary waves depend on not only the ratio of wave height or wavelength to water depth but also both the water-density and layer-thickness ratios among layers, which makes it more difficult to understand the properties of internal waves than those of surface waves.

In the present study, numerical solutions of surface and internal solitary waves are obtained through a new method, where we satisfy advection equations on physical quantities including surface/interface displacements and velocity potential. This method is applied to solve the set of nonlinear wave equations based on a variational principle without any assumptions of wave nonlinearity and dispersion (Kakinuma, 2001). The numerical solutions are compared with the corresponding theoretical solutions of the KdV theory or the shallower version of Choi and Camassa (1999), as well as numerical solutions of the Euler equations (Grue et al., 1997). Properties of surface and internal solitary waves are also discussed in consideration of vertical distribution of horizontal and vertical velocity, as well as kinetic and potential energy.

## NONLINEAR EQUATIONS FOR SURFACE/INTERNAL WAVES

### Nonlinear Equations for Surface and Internal Waves

Illustrated in Fig. 1 is a schematic of a multi-layer system of inviscid and incompressible fluids represented as  $i$  ( $i = 1, 2, \dots, D$ ) from top to bottom. The thickness of the  $i$ -layer is denoted by  $h_i(\mathbf{x})$  in still water. None of the fluids mix even in motion and the density  $\rho_i$  ( $\rho_1 < \rho_2 < \dots < \rho_D$ ) is spatially uniform and temporally constant in each layer.

Fluid motion is assumed to be irrotational, resulting in the existence of velocity potential  $\phi_i$ , which is expanded into a power series of vertical position  $z$  with weightings  $f_{i,\alpha_i}$  as

$$\phi_i(\mathbf{x}, z, t) = \sum_{\alpha=0}^{N_i-1} \{ f_{i,\alpha}(\mathbf{x}, t) \cdot z^{\alpha} \} \equiv f_{i,\alpha_i} \cdot z^{\alpha_i}, \quad (1)$$

where  $N_i$  is number of terms for expanded velocity potential in the  $i$ -layer; the sum rule of product is adopted for subscript  $\alpha_i$ ; the top face of the 1-layer is described by  $z = 0$  in the still water condition.

The nonlinear surface/internal wave equations derived by Kakinuma (2001) based on a variational principle are

$$\begin{aligned} \eta_{i,1}^{\alpha_i} \frac{\partial \eta_{i,1}}{\partial t} - \eta_{i,0}^{\alpha_i} \frac{\partial \eta_{i,0}}{\partial t} + \frac{1}{\alpha_i + \beta_i + 1} \nabla \cdot \{ (\eta_{i,1}^{\alpha_i + \beta_i + 1} - \eta_{i,0}^{\alpha_i + \beta_i + 1}) \nabla f_{i,\beta_i} \} \\ - \frac{\alpha_i \beta_i}{\alpha_i + \beta_i - 1} (\eta_{i,1}^{\alpha_i + \beta_i + 1} - \eta_{i,0}^{\alpha_i + \beta_i + 1}) f_{i,\beta_i} = 0, \end{aligned} \quad (2)$$

<sup>1</sup> International Research Institute of Disaster Science, Tohoku University, 468-1 Aramaki Aza-Aoba, Aoba-ku, Miyagi 980-8579, Japan

<sup>2</sup> Graduate School of Science and Engineering, Kagoshima University, 1-21-40 Korimoto, Kagoshima, Kagoshima 890-0065, Japan

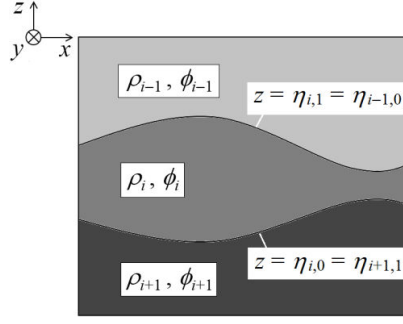


Figure 1. Schematic of a multi-layer system.

$$\eta_{i,j}^{\beta_i} \frac{\partial f_{i,\beta_i}}{\partial t} + \frac{1}{2} \eta_{i,j}^{\beta_i+\gamma_i} \nabla f_{i,\beta_i} \nabla f_{i,\gamma_i} + \frac{1}{2} \beta_i \gamma_i \eta_{i,j}^{\beta_i+\gamma_i-2} f_{i,\beta_i} f_{i,\gamma_i} + g \eta_{i,j} + \frac{P_{i,j} + P_i}{\rho_i} = 0 \quad (j=0 \text{ or } 1), \quad (3)$$

where  $\eta_{i,0}(\mathbf{x}, t)$  and  $\eta_{i,1}(\mathbf{x}, t)$  are displacements of the lower and upper interfaces of the  $i$ -layer, respectively;  $p_{i,0}(\mathbf{x}, t)$  and  $p_{i,1}(\mathbf{x}, t)$  are pressures at the lower and upper interfaces of the  $i$ -layer, respectively;  $g$  is gravitational acceleration;  $P_i = \sum_{k=1}^{i-1} (\rho_i - \rho_k) g h_k$ ;  $\nabla$  is a partial differential operator in the horizontal plane, i.e.,  $\nabla = (\partial/\partial x, \partial/\partial y)$ .

In the present study, the number of terms for expanded velocity potential in every layer is equal, i.e.,  $N_i = N$ .

#### Nonlinear Equations for Surface Waves with a Free Water Surface

Nonlinear equations for surface waves based on the variational principle are obtained by applying Eqs. (2) and (3) to the one-layer problem with a free water surface, where  $i = 1$  and  $j = 1$ , as

$$\zeta^\alpha \frac{\partial \zeta}{\partial t} + \frac{1}{\alpha + \beta + 1} \nabla \{ (\zeta^{\alpha+\beta+1} - b^{\alpha+\beta+1}) \nabla f_\beta \} - \frac{\alpha\beta}{\alpha + \beta - 1} (\zeta^{\alpha+\beta-1} - b^{\alpha+\beta-1}) f_\beta = 0, \quad (4)$$

$$\zeta^\beta \frac{\partial f_\beta}{\partial t} + \frac{1}{2} \zeta^{\beta+\gamma} \nabla f_\beta \nabla f_\gamma + \frac{1}{2} \beta \gamma \zeta^{\beta+\gamma-2} f_\beta f_\gamma + g \zeta = 0, \quad (5)$$

where the surface and bottom profiles are described by  $z = \eta_{1,1} = \zeta(\mathbf{x}, t)$  and  $z = \eta_{1,0} = b(\mathbf{x})$ , respectively.

#### Nonlinear Equations for Internal Waves in a Two-Layer System Covered with a Fixed Horizontal Plate

If we consider a two-layer system covered with a fixed horizontal plate, where  $\eta_{1,1} = 0$  and  $\eta_{2,0} = b(\mathbf{x})$ , then Eqs. (2) and (3) are reduced to

[Upper layer] ( $i = 1$  and  $j = 0$ )

$$\eta^\alpha \frac{\partial \eta}{\partial t} + \frac{1}{\alpha + \beta + 1} \nabla (\eta^{\alpha+\beta+1} \nabla f_{1,\beta}) - \frac{\alpha\beta}{\alpha + \beta - 1} \eta^{\alpha+\beta+1} f_{1,\beta} = 0, \quad (6)$$

$$\eta^\beta \frac{\partial f_{1,\beta}}{\partial t} + \frac{1}{2} \eta^{\beta+\gamma} \nabla f_{1,\beta} \nabla f_{1,\gamma} + \frac{1}{2} \beta \gamma \eta^{\beta+\gamma-2} f_{1,\beta} f_{1,\gamma} + g \eta + \frac{P_{1,0}}{\rho_1} = 0, \quad (7)$$

[Lower layer] ( $i = 2$  and  $j = 1$ )

$$\eta^\alpha \frac{\partial \eta}{\partial t} + \frac{1}{\alpha + \beta + 1} \nabla \{ (\eta^{\alpha+\beta+1} - b^{\alpha+\beta+1}) \nabla f_{2,\beta} \} - \frac{\alpha\beta}{\alpha + \beta - 1} (\eta^{\alpha+\beta-1} - b^{\alpha+\beta-1}) f_{2,\beta} = 0, \quad (8)$$

$$\eta^\beta \frac{\partial f_{2,\beta}}{\partial t} + \frac{1}{2} \eta^{\beta+\gamma} \nabla f_{2,\beta} \nabla f_{2,\gamma} + \frac{1}{2} \beta \gamma \eta^{\beta+\gamma-2} f_{2,\beta} f_{2,\gamma} + g \eta + \frac{1}{\rho_2} \{ p_{2,1} + (\rho_2 - \rho_1) g h_1 \} = 0, \quad (9)$$

where the interface profile is described by  $z = \eta(\mathbf{x}, t)$ ;  $\eta = \eta_{1,0} = \eta_{2,1}$ . Equations (7) and (9) lead to

$$\eta^\beta \frac{\partial f_{2,\beta}}{\partial t} + \frac{1}{2} \eta^{\beta+\gamma} \nabla f_{2,\beta} \nabla f_{2,\gamma} + \frac{1}{2} \beta \gamma \eta^{\beta+\gamma-2} f_{2,\beta} f_{2,\gamma} + g(\eta + h_1) - \frac{\rho_1}{\rho_2} \left\{ \eta^\beta \frac{\partial f_{1,\beta}}{\partial t} + \frac{1}{2} \eta^{\beta+\gamma} \nabla f_{1,\beta} \nabla f_{1,\gamma} + \frac{1}{2} \beta \gamma \eta^{\beta+\gamma-2} f_{1,\beta} f_{1,\gamma} + g(\eta + h_1) \right\} = 0, \quad (10)$$

for  $p_{1,0}$  equals  $p_{2,1}$ .

### Nonlinear Equations for Permanent Waves Traveling at a Constant Celerity

We consider waves progressing at a constant celerity with no deformation of waveform, such that the advection equations written by  $\partial F / \partial t = -C \partial F / \partial x$  are satisfied, where  $C$  is the constant celerity; the physical quantities  $F$  are surface and interface displacements, velocity, velocity potential, etc. By substituting the advection equations into the nonlinear wave equations presented above, the time-derivative terms are eliminated: for example, the advection equations are substituted into Eqs. (4) and (5), we obtain nonlinear equations for surface waves traveling at celerity  $C$  without deformation of waveform as

$$-C \zeta^\alpha \nabla \zeta + \frac{1}{\alpha + \beta + 1} \nabla \{ (\zeta^{\alpha+\beta+1} - b^{\alpha+\beta+1}) \nabla f_\beta \} - \frac{\alpha \beta}{\alpha + \beta - 1} (\zeta^{\alpha+\beta-1} - b^{\alpha+\beta-1}) f_\beta = 0, \quad (11)$$

$$-C \zeta^\beta \nabla f_\beta + \frac{1}{2} \zeta^{\beta+\gamma} \nabla f_\beta \nabla f_\gamma + \frac{1}{2} \beta \gamma \zeta^{\beta+\gamma-2} f_\beta f_\gamma + g \zeta = 0. \quad (12)$$

### NUMERICAL CALCULATION METHOD

In the calculation process of nonlinear equations for permanent waves progressing at a constant celerity, the Newton-Raphson method is applied to find convergent solutions using suitable initial values with lateral boundary conditions. In the present study, numerical solutions of surface and internal solitary waves are obtained through this method. The process to obtain numerical solutions of surface solitary waves using Eqs. (11) and (12) is as follows:

First, we get a set of solitary-wave solutions of the KdV theory, i.e., surface displacement  $\zeta_{\text{KdV}}$ , celerity  $C_{\text{KdV}}$ , and velocity potential  $\phi_{\text{KdV}}$ . It should be noted that both the wave height and wave celerity should be small enough in order to obtain more appropriate solutions. The weightings  $f_{\alpha, \text{KdV}}$  for expanded velocity potential  $\phi_{\text{KdV}}$  can be evaluated by solving the equation of continuity, i.e., Eq. (11), which becomes a linear equation after  $\zeta_{\text{KdV}}$  and  $C_{\text{KdV}}$  are substituted into it.

Second, we solve Eqs. (11) and (12) using  $\zeta_{\text{KdV}}$  and  $f_{\alpha, \text{KdV}}$  as the initial values in the Newton-Raphson method, where the celerity  $C$  equals  $C_1 = C_{\text{KdV}}$ , to obtain the first numerical solutions, i.e.,  $\zeta_1$  and  $f_{\alpha, 1}$ .

Third, we solve Eqs. (11) and (12) using  $\zeta_1$  and  $f_{\alpha, 1}$  as the initial values in the Newton-Raphson method, where the celerity  $C$  equals  $C_2 = C_1 + \varepsilon$ , to obtain the next numerical solutions, i.e.,  $\zeta_2$  and  $f_{\alpha, 2}$ . Note that  $\varepsilon / C_1$  can take a value between  $1.0^{-5}$  and  $1.0^{-3}$ .

By repeating the process with celerity  $C$  increased step by step, we obtain numerical solutions of  $\zeta$  and  $f_\alpha$  for surface solitary waves progressing at any celerity  $C$ .

The method proposed above is expected to be applicable to not only Eqs. (11) and (12) but also Eqs. (6), (8), and (10), as well as other wave equations such as Boussinesq-type equations, to obtain numerical solutions of surface/internal solitary waves.

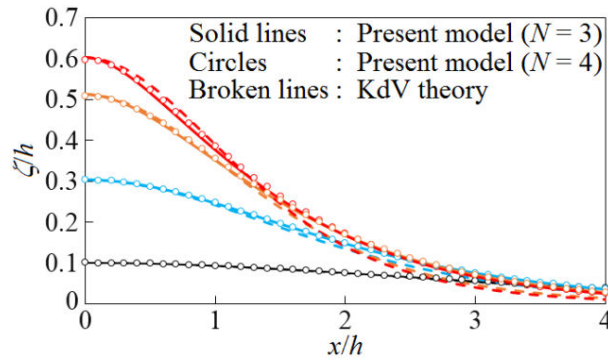
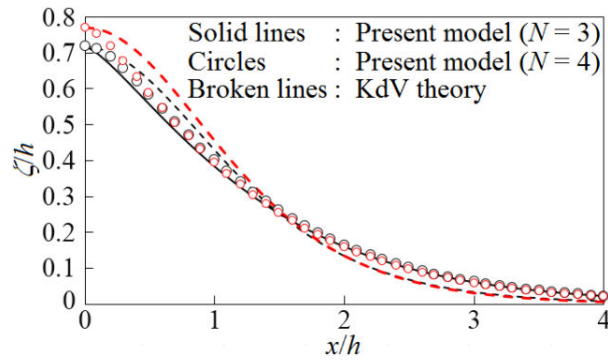
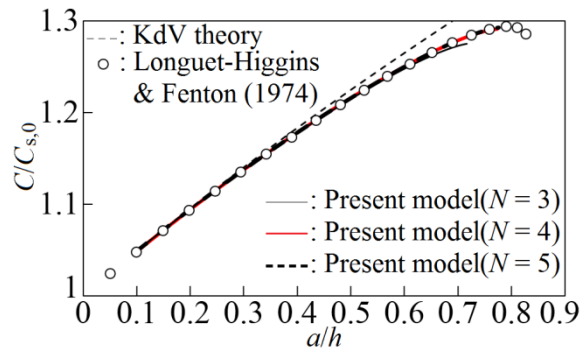
(a)  $a/h = 0.1, 0.3, 0.51, \text{ and } 0.6$ (b)  $a/h = 0.72 \text{ and } 0.77$ 

Figure 2. Water surface profiles of surface solitary waves.

Figure 3. Relative celerity of surface solitary waves, where  $C_{s,0}$  is celerity of linear surface waves in shallow water.

## SURFACE SOLITARY WAVES

### Comparison of Solutions

Numerical solutions of surface solitary waves obtained through the present method are compared with the corresponding KdV solutions. The number of terms for expanded velocity potential,  $N$ , is equal to 3, 4, or 5. The total length of the calculation domain along the horizontal axis  $x$ ,  $L$ , and the grid width for computation,  $\Delta x$ , are  $50h$  and  $0.02h$ , respectively, where  $h$  is still water depth.

Shown in Fig. 2 are calculation results of surface profiles compared with the corresponding KdV solutions. The surface profiles obtained through the present method are steeper than the KdV solutions around the peaks when the ratio of wave amplitude to still water depth,  $a/h$ , is large. In the simulation, the maximum value of  $a/h$  is 0.77 when  $N > 3$ ; it is difficult to generate such a solitary wave of large amplitude in usual hydraulic experiments.

Figure 3 compares the relative wave celerity  $C/C_{s,0}$  obtained using the present method with that of the KdV theory, as well as the corresponding numerical solution through Longuet-Higgins and Fenton (1974), where  $C$  is celerity of surface solitary waves, while  $C_{s,0}$  is celerity of linear waves in shallow

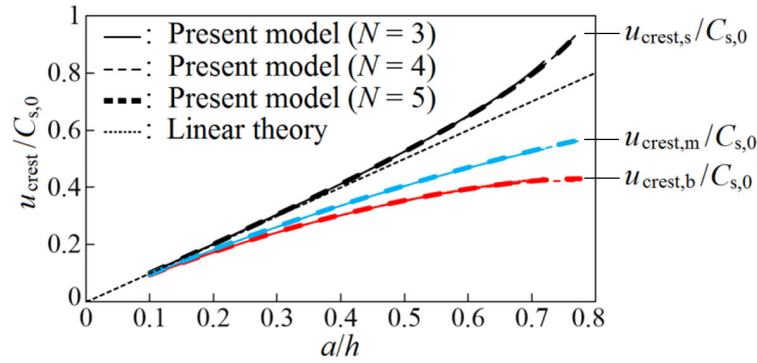


Figure 4. Relative horizontal velocity at the location of crest, where the subscripts s, b, and m of horizontal velocity denote the values at the surface, at the bottom, and averaged vertically, respectively.

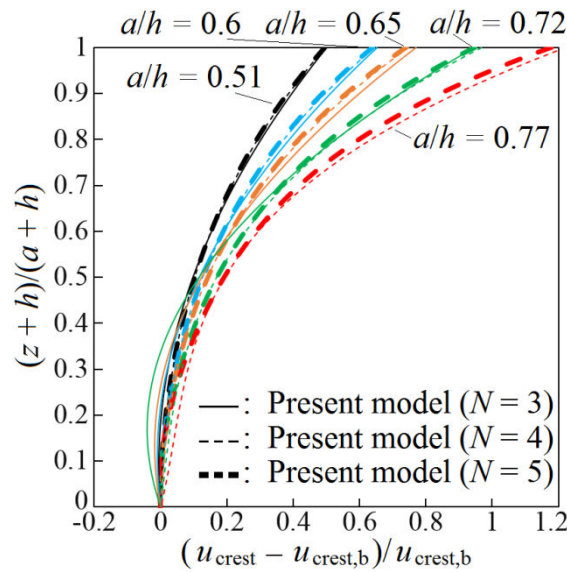


Figure 5. Vertical distribution of relative horizontal velocity at the location of crest of surface solitary waves.

water, i.e.,  $\sqrt{gh}$ . The value of  $C/C_{s,0}$  through the present method is almost equal to that by Longuet-Higgins and Fenton when  $N > 3$ , which shows the high accuracy of the present results.

#### Velocity at the Location of Crest

Shown in Fig. 4 are three values of water particle velocity at the location of crest,  $u_{crest}$ :  $u_{crest,s}$  at the water surface,  $u_{crest,b}$  at the bottom, and  $u_{crest,m}$ , i.e., mean velocity defined as

$$u_{crest,m} = \frac{1}{h+a} \int_{-h}^{\zeta} u_{crest} dz. \quad (13)$$

The dashed line in Fig. 4 represents the theoretical solution of the linear shallow water theory, i.e.,  $C_{s,0}a/h$ . According to the figure, the difference between  $u_{crest,s}$  and  $u_{crest,b}$  becomes larger as  $a/h$  is larger. When  $a/h$  equals 0.77,  $u_{crest,s}$  is 1.7 and 2.2 times as large as  $u_{crest,m}$  and  $u_{crest,b}$ , respectively.

Figure 5 shows vertical distribution of horizontal velocity at the location of crest,  $u_{crest}$ , where  $a/h = 0.51, 0.6, 0.65, 0.72,$  and  $0.77$ . The vertical distribution of  $u_{crest}/u_{crest,b}$  shows larger curvature as  $a/h$  is larger. Such velocity distribution of large curvature cannot be reproduced with wave models considering only weak dispersion (Fujima et al., 1985).

#### Wave Energy of Surface Solitary Waves

Wave energy of surface solitary waves per unit width is evaluated by

$$E_{s,p} = \int_{-L/2}^{L/2} \int_0^{\zeta} \rho g z dz dx / \rho g h^3, \quad (14)$$

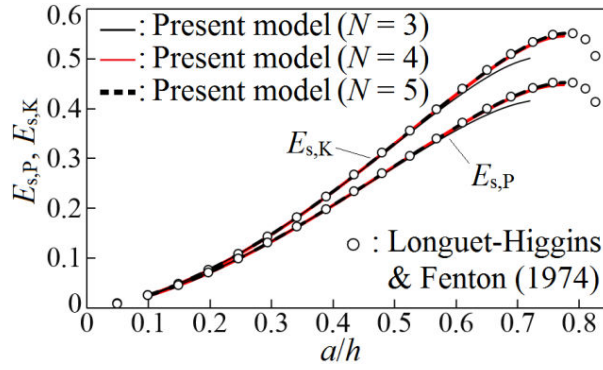


Figure 6. Potential energy  $E_{s,P}$  and kinetic energy  $E_{s,K}$  of surface solitary waves.

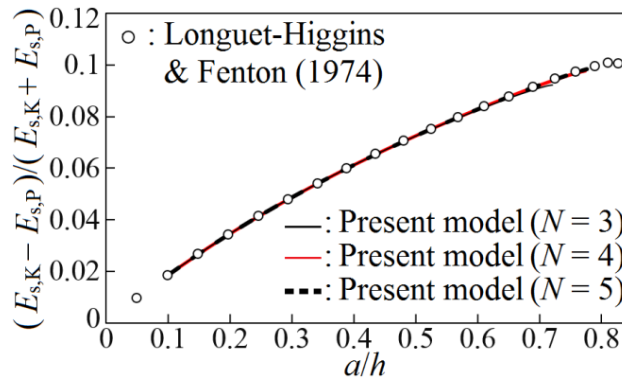


Figure 7. Ratio of difference between kinetic and potential energy to total energy of surface solitary waves.

$$E_{s,K} = \int_{-L/2}^{L/2} \int_{-h}^{\zeta} \frac{1}{2} \rho \left\{ (\nabla \phi)^2 + \left( \frac{\partial \phi}{\partial z} \right)^2 \right\} dz dx / \rho g h^3, \quad (15)$$

$$E_s = E_{s,P} + E_{s,K}, \quad (16)$$

where  $E_{s,P}$ ,  $E_{s,K}$ , and  $E_s$  are potential energy, kinetic energy, and total energy, respectively.

The relationship between wave energy and  $a/h$  is shown in Fig. 6. When  $N = 3$ , the difference between the numerical solutions through the present method and the results by Longuet-Higgins and Fenton (1974) becomes larger as  $a/h$  is larger. On the other hand, when  $N = 4$  and 5, the wave energy through the present method is in good agreement with that by Longuet-Higgins and Fenton owing to the accurate water surface displacement and velocity obtained through the present method. If  $a/h > 0.77$ , however, the solutions cannot be found through the present method with the calculation conditions mentioned above even when  $N = 5$ .

As Fig. 7 indicates, the ratio of difference between  $E_{s,K}$  and  $E_{s,P}$  to total energy ( $E_{s,K} + E_{s,P}$ ) becomes larger as  $a/h$  is larger when  $a/h < 0.77$ .

## INTERNAL SOLITARY WAVES

### Comparison of Solutions

Numerical solutions of internal solitary waves obtained using the present method are compared with the corresponding solutions of the KdV theory, as well as those through the shallower version of Choi and Camassa (1999), which is a fully nonlinear theory, for the assumption of order is that  $O(a/h) = 1$  and  $O((h/\lambda)^4) \ll 1$ , where  $a$ ,  $h$ , and  $\lambda$  are representative values of wave amplitude, water depth, and wavelength, respectively. Introduced in Appendix are the solutions of interface displacement and wave celerity presented by Choi and Camassa (1999) for shallower conditions. The deeper version derived by Choi and Camassa (1999) is not applied in the present paper.

In Figs. 8 (a) – (e), interface profiles obtained through the present method are compared with the KdV solutions, as well as the results through the shallower version of Choi and Camassa, where  $h$  is

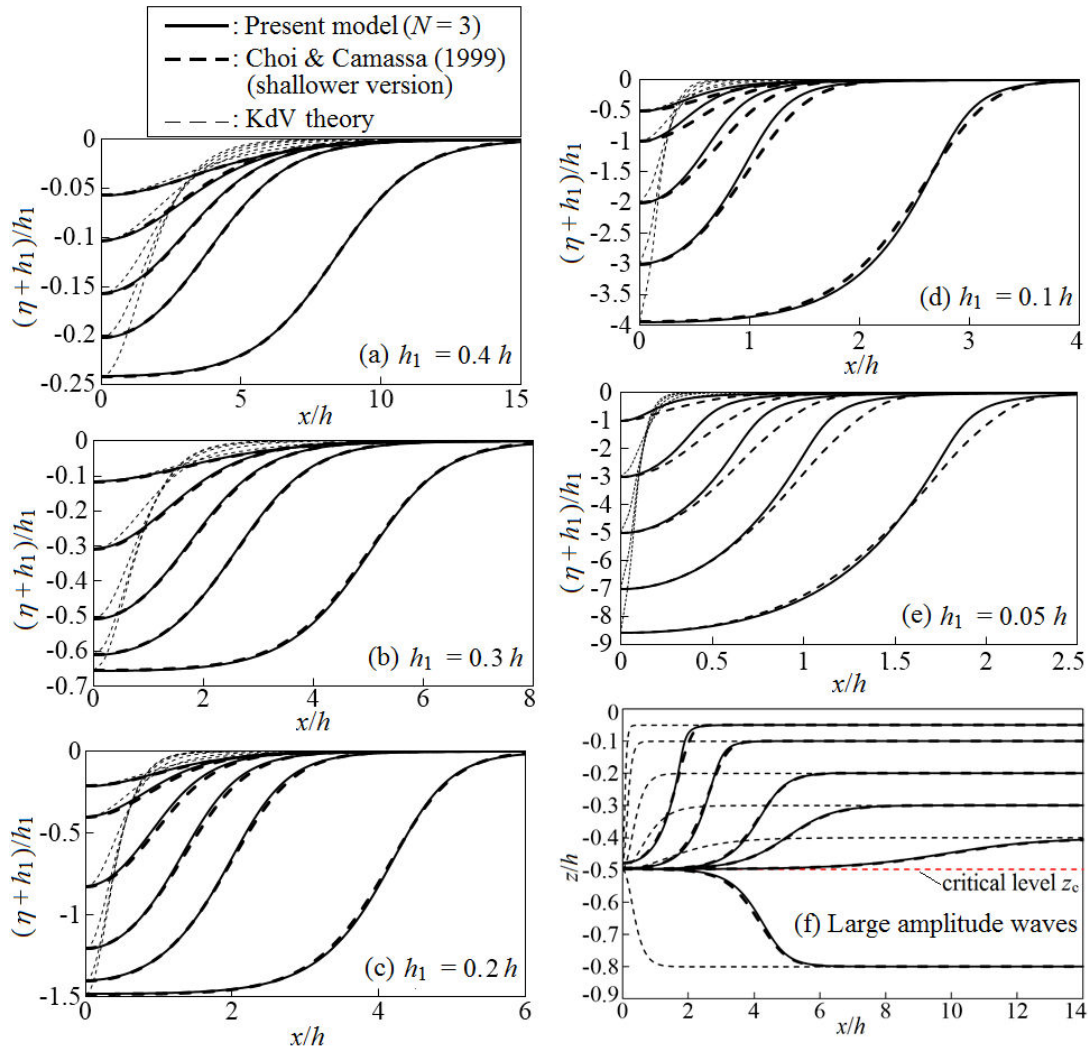


Figure 8. Interface profiles of internal solitary waves, where  $h_1$  is thickness of the upper layer in still water.

total water depth and  $h_1$  is thickness of the upper layer in still water; the density ratio  $\rho_2/\rho_1$  equals 1.02; the number of terms for expanded velocity potential,  $N$ , is equal to three. The interface profiles through the present method, as well as those by Eq. (A-1) of Choi and Camassa, become flatter as the trough is closer to the critical level, which cannot be passed by an interface of a stable internal wave (Funakoshi and Oikawa, 1986). In cases  $h_1/h$  equals 0.1 and 0.05, as shown in Figs. 8 (d) and (e), respectively, the interface profiles by Eq. (A-1) disagree with those through the present method.

Shown in Fig. 8 (f) are interface profiles with large amplitude very close to the difference between the critical level and the level of interface in still water, where the results obtained using Eq. (A-1) and the present method are in good agreement.

Figures 9 (a) – (e) show the relationship between relative wavelength  $\lambda_l/h$  and ratio of wave amplitude to upper layer thickness in still water,  $|a|/h_1$ , where the wavelength is defined by  $\lambda_l = \int_{-\infty}^{\infty} (\eta + h_1) dx / a$ . The relative wavelength  $\lambda_l/h$  through the KdV theory shows monotone decrease as  $|a|/h_1$  becomes larger, where it is assumed that  $O(a/h) = O((h/\lambda)^2)$ . On the other hand, the relative wavelength  $\lambda_l/h$  through the present method, as well as that of the shallower version of Choi and Camassa, has a minimal value, which means that the interface profile is steeper as  $|a|/h_1$  is medium.

The relative wavelength  $\lambda_l/h$  of the shallower version of Choi and Camassa is larger than that through the present method when  $h_1/h$  is smaller and  $|a|/h_1$  is medium. In case  $h_1/h$  equals 0.05, as shown in Fig. 9 (e), the shallower version of Choi and Camassa is not applicable to internal solitary waves with strong dispersion attributed to large  $O((h/\lambda)^4)$  when  $|a|/h_1$  is medium, although  $O((h/\lambda)^4)$  is small when  $|a|/h_1$  is small enough, or large enough resulting in the good agreement of the results

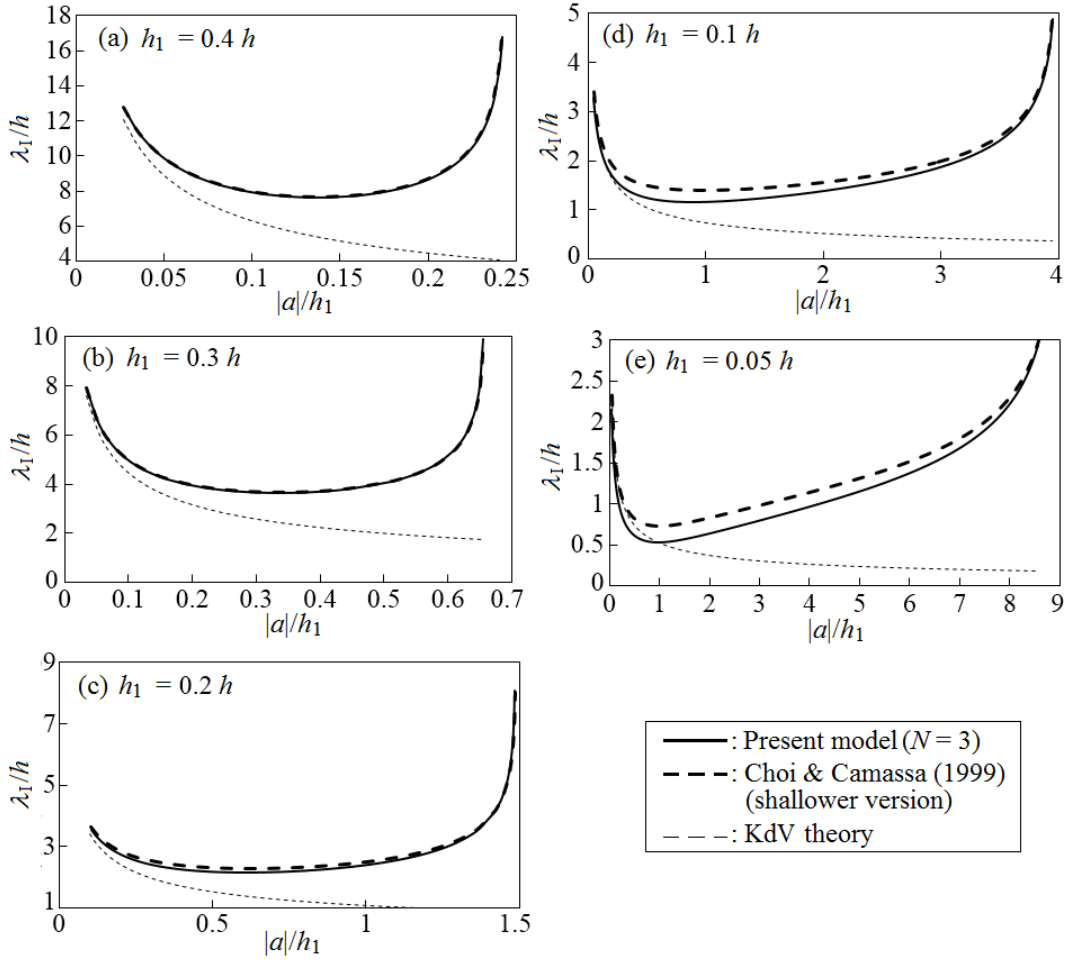


Figure 9. Relationship between relative wavelength of internal solitary waves and ratio of amplitude to thickness of the upper layer in still water.

through the two models as shown in Fig. 8 (f).

Figure 10 shows the relationship between relative wave celerity  $C/C_{i,0}$  and  $|a|/h_1$ , where  $C_{i,0}$  is celerity of linear internal waves in shallow water. In comparison with the results obtained through the present method, the KdV theory overestimates  $C/C_{i,0}$  except when  $|a|/h_1$  is small, while the shallower version of Choi and Camassa overestimates it slightly when  $|a|/h_1$  is medium.

The relationship between half of relative wavelength,  $0.5\lambda_1/h_2$ , and ratio of wave amplitude to lower layer thickness in still water,  $a/h_2$ , is shown in Fig. 11, where  $\lambda_1 = \int_{-\infty}^{\infty} (\eta + h_1) dx / a$ . The values of  $0.5\lambda_1/h_2$  through the present method are in good agreement with the results obtained by Grue et al. (1997), where the Euler equations were solved numerically.

#### Velocity at the Location of Trough

In Fig. 12, interface profiles obtained through the present method are drawn with a critical level, where the thickness of the upper and lower layers is 0.15 m and 0.62 m, respectively, in still water; the fluid density in the upper and lower layers is  $999.0 \text{ kg/m}^3$  and  $1022.0 \text{ kg/m}^3$ , respectively. The relative amplitude of the internal solitary waves,  $|a|/h_1$ , is 0.36 and 1.35; in the latter case, the amplitude is close to the upper limit of amplitude,  $a_{\max}$ , evaluated by

$$a_{\max} = \frac{h_2 \rho_1^{1/2} - h_1 \rho_2^{1/2}}{\rho_1^{1/2} + \rho_2^{1/2}}, \quad (17)$$

where the amplitude in the latter case is about 0.20 m, while the upper limit is about 0.23 m.

Shown in Fig. 13 are vertical distributions of  $u/C_{i,0}$  at the location of trough of the internal solitary waves shown in Fig. 12, i.e.,  $x/h = 0$ , where the relative horizontal velocity  $u/C_{i,0}$  through the present

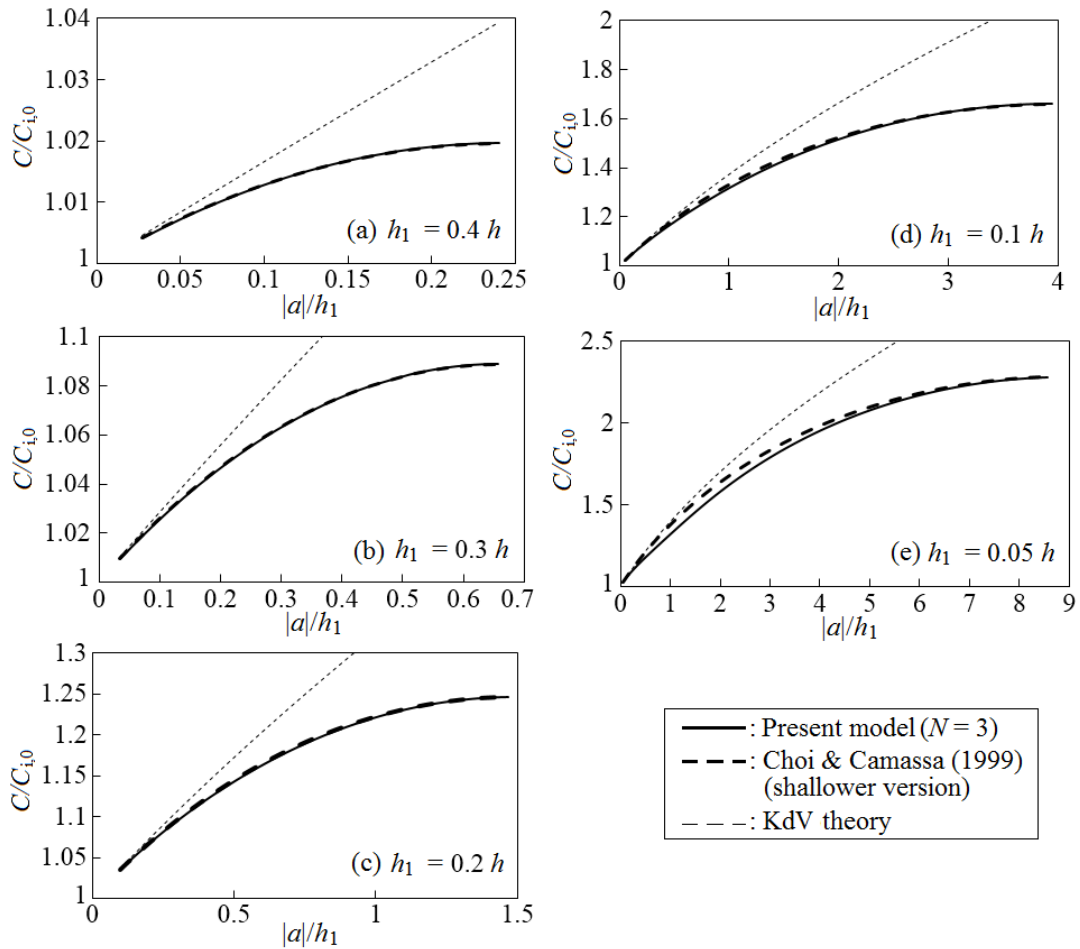


Figure 10. Relative celerity of internal solitary waves, where  $C_{i,0}$  is celerity of linear internal waves in shallow water.

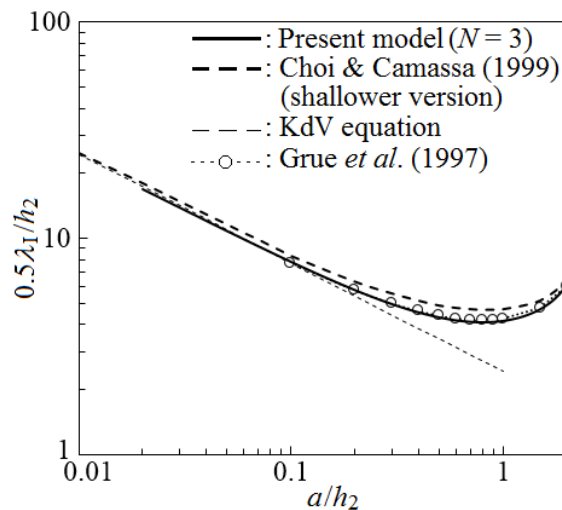


Figure 11. Relationship between half of relative wavelength of internal solitary waves and ratio of amplitude to thickness of the lower layer in still water.

method is compared with the experimental data obtained by Grue et al. (1999). According to Fig. 13, the numerical solutions through the proposed method are in harmony with the experimental results.

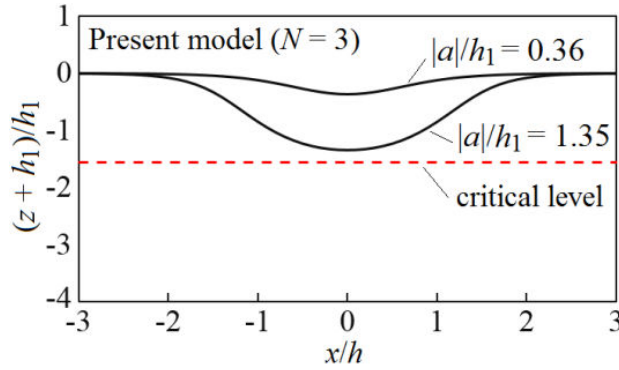


Figure 12. Interface profiles of two internal solitary waves, where  $\rho_1 = 999.0 \text{ kg/m}^3$ ,  $\rho_2 = 1022.0 \text{ kg/m}^3$ ,  $h_1 = 0.15 \text{ m}$ , and  $h_2 = 0.62 \text{ m}$ .

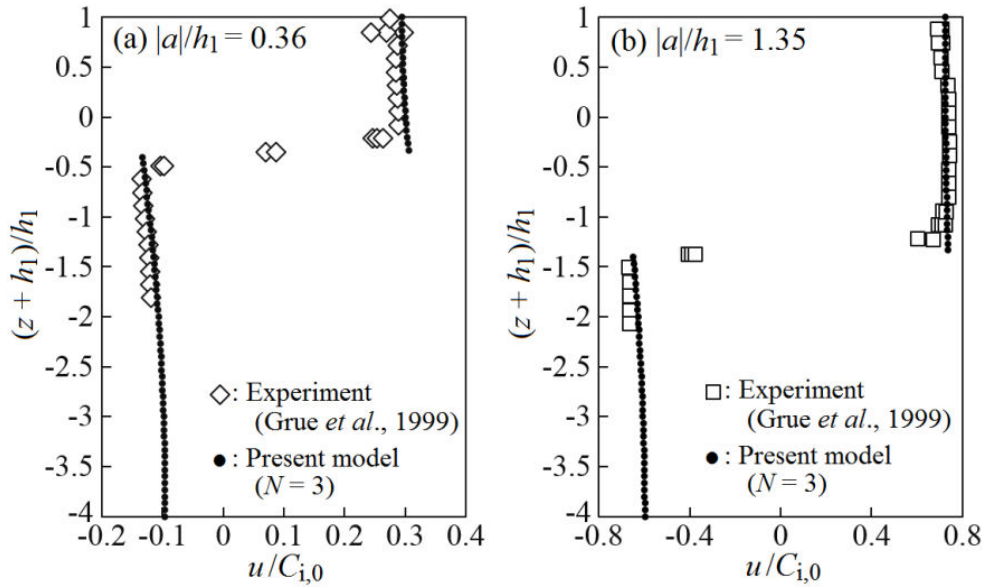


Figure 13. Vertical distribution of relative horizontal velocity at the location of trough of the internal solitary waves shown in Fig. 12.

Distributions of relative horizontal velocity  $u/C$  and relative vertical velocity  $w/C$  are shown in Figs. 14 (a) and (b), respectively, where  $h_1/h = 0.2$  and  $|a|/h_1 = 1.4$ . The maximum values of  $u/C$  and  $w/C$  are about 0.6 and 0.2, respectively, in the present case.

Figure 15 shows  $(u_{1,\max} - u_{1,b})/u_{1,\max}$ , where  $u_{1,\max}$  and  $u_{1,b}$  are the values of horizontal velocity at the interface and the upper boundary, i.e., the top face, respectively, in the upper layer at the location of trough. When  $|a|/a_{\max}$  is close to zero or one, the value of  $(u_{1,\max} - u_{1,b})/u_{1,\max}$  is around zero. The same is true of  $(u_{2,\min} - u_{2,b})/u_{2,\min}$  as shown in Fig. 16, where  $u_{2,\min}$  and  $u_{2,b}$  are the values of horizontal velocity at the interface and the bottom, respectively, in the lower layer at the location of trough. Thus the vertical distribution of horizontal velocity is approximately uniform in both the upper and lower layers when the amplitude is close to zero or the upper limit  $a_{\max}$ .

#### Wave Energy of Internal Solitary Waves

Wave energy of internal solitary waves per unit width is evaluated by

$$E_{i,p} = \int_{-L/2}^{L/2} \frac{1}{2} (\rho_2 - \rho_1) g (\eta + h_1)^2 dx \Big/ (\rho_2 - \rho_1) g h^3, \quad (18)$$

$$E_{i,K} = \left\{ \int_{-L/2}^{L/2} \int_{-h}^0 \frac{1}{2} \rho_i \left[ (\nabla \phi_i)^2 + \left( \frac{\partial \phi_i}{\partial z} \right)^2 \right] dz dx \right\} \Big/ (\rho_2 - \rho_1) g h^3, \quad (19)$$

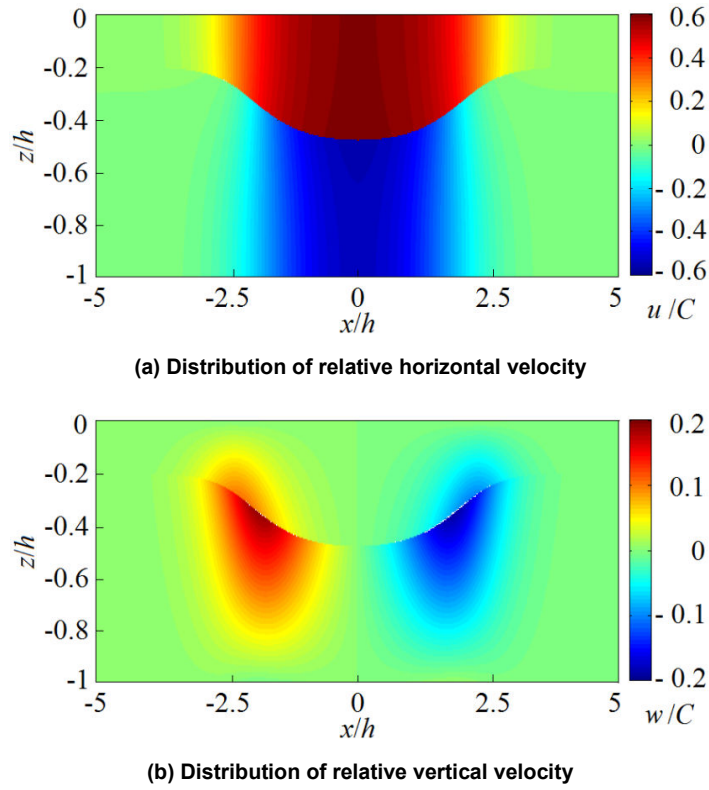


Figure 14. Distribution of relative velocity, where  $h_1/h = 0.2$  and  $|a|/h_1 = 1.4$ ;  $C$  is celerity of internal solitary waves.

$$E_i = E_{i,p} + E_{i,k}, \quad (20)$$

where  $E_{i,p}$ ,  $E_{i,k}$ , and  $E_i$  are available potential energy, kinetic energy, and total energy of internal solitary waves.

According to Fig. 17, which shows the relative energy difference, i.e., the ratio of difference between kinetic energy and available potential energy to total energy,  $(E_{i,k} - E_{i,p})/(E_{i,k} + E_{i,p})$ , the relative energy difference is large when  $h_1/h$  is small or  $|a|/a_{\max}$  is medium. On the other hand, if the wave amplitude is close to zero or the upper limit  $a_{\max}$ , then the relative energy difference is small; hence it follows that internal solitary waves of large amplitude show the characteristic similar to that of linear waves in terms of the relative energy difference, which is zero for linear waves, although the linear theory makes no mention of such internal waves of large amplitude.

## NUMERICAL SIMULATION OF SOLITARY WAVES TRAVELING OVER A HORIZONTAL BOTTOM

### Propagation of a Surface Solitary Wave

Numerical simulation of propagation of surface/internal solitary waves over a horizontal bottom has also been performed using the time-dependent numerical model (Yamashita et al., 2013). In the calculation process of wave propagation, the time development is carried out by applying implicit schemes similar to that of Nakayama and Kakinuma (2010).

A progressive surface solitary wave of large amplitude is depicted in Fig. 18, with an almost permanent waveform obtained by giving numerical solutions through the method proposed above as the initial conditions to solve Eqs. (4) and (5). The calculation conditions are as follows:  $a/h=0.66$ ,  $N=3$ ,  $\Delta x/h=0.1$ , and  $C_{s,0} \Delta t/\Delta x=0.003$ , where  $a$ ,  $h$ ,  $N$ , and  $C_{s,0}$  are amplitude, still water depth, number of terms for expanded velocity potential, and celerity of linear surface waves in shallow water, respectively;  $\Delta x$  and  $\Delta t$  are grid width and time-step interval for computation, respectively.

### Propagation of an Internal Solitary Wave

Shown in Fig. 19 is a progressive internal solitary wave obtained by solving Eqs. (6), (8), and (10) with the initial conditions through the proposed method. The calculation conditions are as follows:

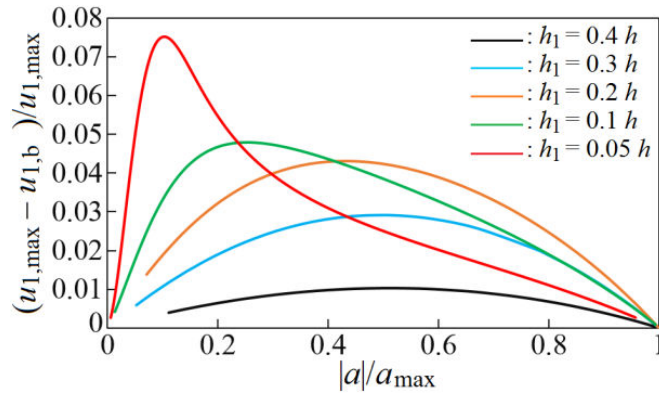


Figure 15. Ratio of difference between horizontal velocities at the interface and top face in the upper layer at the location of trough, where  $a_{\max}$  defined by Eq. (17) is the upper limit of amplitude of internal solitary waves.

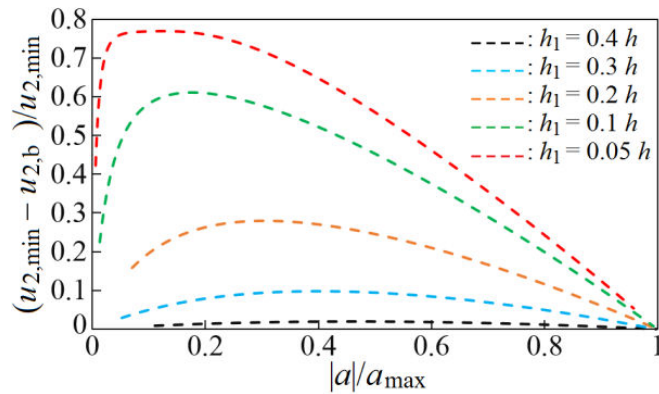


Figure 16. Ratio of difference between horizontal velocities at the interface and bottom in the lower layer at the location of trough, where  $a_{\max}$  defined by Eq. (17) is the upper limit of amplitude of internal solitary waves.

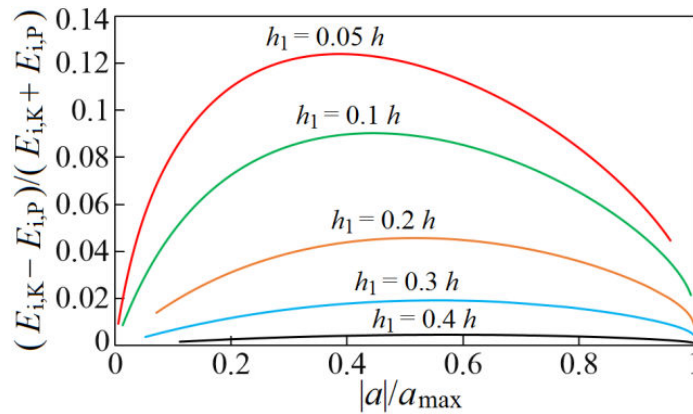


Figure 17. Ratio of difference between kinetic energy and available potential energy to total energy, where  $a_{\max}$  defined by Eq. (17) is the upper limit of amplitude of internal solitary waves.

$\rho_2/\rho_1=1.02$ ,  $h_1/h=0.2$ ,  $|a|/h_1=1.4$ ,  $N=3$ ,  $\Delta x/h=0.1$ , and  $C_{i,0} \Delta t/\Delta x=0.018$ , where  $\rho_1$  and  $\rho_2$  are fluid density in the upper and lower layers, respectively;  $h_1$  and  $h$  are thickness of the upper layer in still water and total water depth, respectively;  $a$ ,  $N$ , and  $C_{i,0}$  are amplitude, number of terms for expanded velocity potential, and celerity of linear internal waves in shallow water, respectively;  $\Delta x$  and  $\Delta t$  are grid width and time-step interval for computation, respectively. The waveform of the internal solitary wave is almost permanent with large amplitude in the neighborhood of the upper limit of amplitude, i.e.,  $|a_{\max}| \approx 1.49h_1$ , such that the interface profile shows a flattend trough.

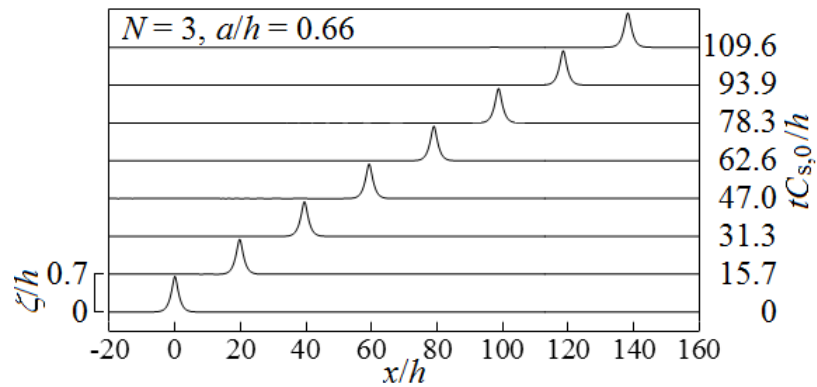


Figure 18. Time variation of water surface profile of a progressive surface solitary wave.

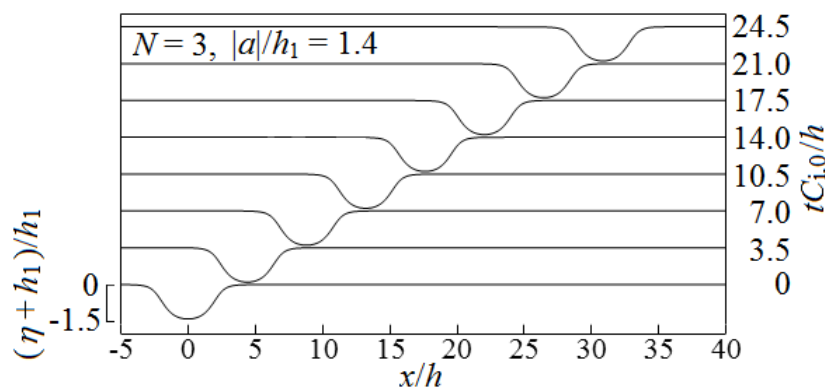


Figure 19. Time variation of interface profile of a progressive internal solitary wave, where  $\rho_2/\rho_1 = 1.02$ ;  $h_1/h = 0.2$ .

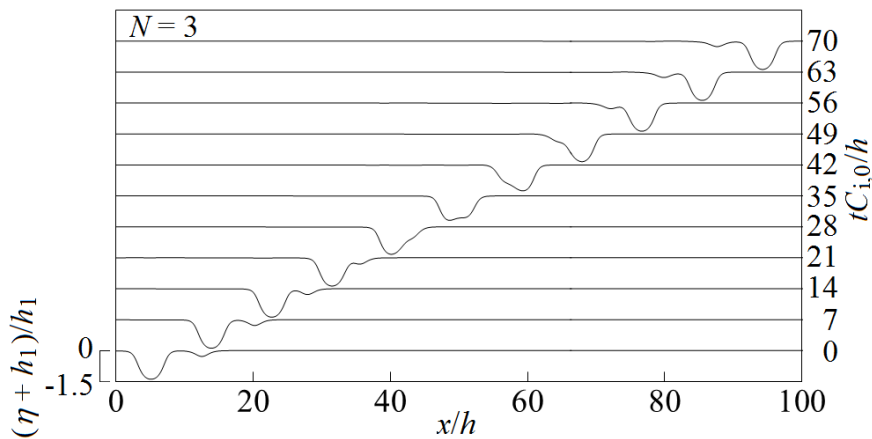


Figure 20. Time variation of interface profile in an overtaking process of two internal solitary waves, where  $\rho_2/\rho_1 = 1.02$ ;  $h_1/h = 0.2$ ;  $|a|/h_1 = 1.4$  and  $0.3$ .

**Interaction between Internal Solitary Waves**

Nonlinear interaction between internal solitary waves is also simulated as shown in Fig. 20, where the initial amplitude of these two waves,  $|a|$ , is  $1.4h_1$  and  $0.3h_1$ ; the other calculation conditions are the same as those in the above-described simulation of propagation of the internal solitary wave. In the overtaking process, the larger internal wave decreases its amplitude owing to nonlinear interaction with the smaller one.

## CONCLUSIONS

The new method has been proposed to obtain numerical solutions of surface and internal solitary waves, where we solve advection equations on physical quantities including surface/interface displacements and velocity potential to find convergent solutions by applying the Newton-Raphson method. The nonlinear wave equations derived using the variational principle were adopted as the fundamental equations. The surface and internal solitary waves obtained through the proposed method were compared with the corresponding theoretical solutions, as well as the numerical solutions of the Euler equations, to verify the accuracy of the solutions through the present method especially for the internal solitary waves of large amplitude traveling at the large celerity with the flattened wave profile.

In the cases of surface solitary waves, the maximum value of the ratio of wave amplitude to still water depth was equal to 0.77 with the present calculation conditions. The surface profile obtained using the present method was steeper than that through the KdV theory around the peak when the ratio of wave amplitude to still water depth was large. The vertical distribution of horizontal velocity at the location of crest showed larger curvature as the ratio of wave amplitude to still water depth was larger.

In the cases of internal solitary waves, the distribution of horizontal velocity was approximately uniform in both the upper and lower layers when the amplitude was close to zero or the upper limit of amplitude of internal solitary waves. When the amplitude was close to zero or the upper limit, the relative difference between the kinetic and potential energy was small, which meant that the internal solitary waves of large amplitude showed the characteristic similar to that of linear waves in terms of the relative energy difference.

The progressive surface and internal solitary waves were also numerically simulated using the time-dependent model, resulting in the propagation of waves with the almost permanent waveforms. In the overtaking process of the two internal solitary waves of different amplitude, the larger wave decreased its amplitude owing to the nonlinear interaction with the smaller one.

## APPENDIX

The solutions of spatial derivative of interface displacement,  $\partial\eta/\partial x$ , and wave celerity  $C$  in two-layer systems presented by Choi and Camassa (1999) for shallower conditions are

$$\left(\frac{\partial\eta}{\partial x}\right)^2 = \left[ \frac{3g(\rho_2 - \rho_1)}{C^2(\rho_1 h_1^2 - \rho_2 h_2^2)} \right] \frac{\eta^2(\eta - a_-)(\eta - a_+)}{(\eta - a_*)}, \quad (\text{A-1})$$

$$a_* = -\frac{h_1 h_2 (\rho_1 h_1 + \rho_2 h_2)}{\rho_1 h_1^2 - \rho_2 h_2^2}, \quad (\text{A-2})$$

$$a_{\pm} = -\frac{1}{2}q_1 \pm \sqrt{\frac{1}{4}q_1^2 - q_2}, \quad (\text{A-3})$$

$$q_1 = -\frac{C^2}{g} - h_1 + h_2, \quad (\text{A-4})$$

$$q_2 = h_1 h_2 \left( \frac{C^2}{C_{i,0}^2} - 1 \right), \quad (\text{A-5})$$

$$\frac{C^2}{C_{i,0}^2} = \frac{(h_1 - a)(h_2 + a)}{h_1 h_2 - (C_{i,0}^2/g)a}, \quad (\text{A-6})$$

$$C_{i,0}^2 = \frac{gh_1 h_2 (\rho_2 - \rho_1)}{\rho_1 h_2 + \rho_2 h_1}, \quad (\text{A-7})$$

where  $g$  is gravitational acceleration;  $\rho_1$  and  $\rho_2$  are fluid density in the upper and lower layers, respectively;  $h_1$  and  $h_2$  are thickness of the upper and lower layers in still water, respectively;  $a$  is wave amplitude;  $C_{i,0}$  is celerity of linear internal waves in shallow water.

## REFERENCES

Choi, W. and R. Camassa. 1999. Fully nonlinear internal waves in a two-fluid system, *Journal of Fluid Mechanics*, 396, 1-36.

- Duda, T. F., J. F. Lynch, J. D. Irish, R. C. Beardsley, S. R. Ramp, C.-S. Chiu, T. Y. Tang and Y.-J. Yang. 2004. Internal tide and nonlinear internal wave behavior at the continental slope in the northern south China Sea, *IEEE Journal of Oceanic Engineering*, 29, 1105-1130.
- Fujima, K., C. Goto and N. Shuto. 1985. Accuracy of nonlinear dispersive long wave equations, *Coastal Engineering in Japan*, 28, 15-30.
- Funakoshi, M. and M. Oikawa. 1986. Long internal waves of large amplitude in a two-layer fluid, *Journal of the Physical Society of Japan*, 55, 128-144.
- Grue, J., H. A. Friis, E. Palm and P. O. Rusan. 1997. A method for computing unsteady fully nonlinear interfacial waves, *Journal of Fluid Mechanics*, 351, 223-252.
- Grue, J., A. Jensen, P.-O. Rusan and J. K. Sveen. 1999. Properties of large-amplitude internal waves, *Journal of Fluid Mechanics*, 380, 257-278.
- Kakinuma, T. 2001. A set of fully nonlinear equations for surface and internal gravity waves, *Proceedings of 5<sup>th</sup> International Conference on Computer Modelling of Seas and Coastal Regions*, WIT Press, 225-234.
- Longuet-Higgins, M. S. and J. D. Fenton. 1974. On the mass, momentum, energy and circulation of a solitary wave. II, *Proceedings of the Royal Society of London. Series A*, 340, 471-493.
- Nakayama, K. and T. Kakinuma. 2010. Internal waves in a two-layer system using fully nonlinear internal-wave equations, *International Journal for Numerical Methods in Fluids*, 62, 574-590.
- Stanton, T. P. and L. A. Ostrovsky. 1998. Observations of highly nonlinear internal solitons over the continental shelf, *Geophysical Research Letters*, 25, 2695-2698.
- Yamashita, K., T. Kakinuma and K. Nakayama. 2013. Shoaling of nonlinear internal waves on a uniformly sloping beach, *Proceedings of 33<sup>rd</sup> International Conference on Coastal Engineering*, ASCE, waves.72, 13 pages.